Intrinsic instability of thin liquid films on nanostructured surfaces

L. Sun,[1,a)] H. Hu,[2,a)] A. A. Rokoni,[2] and Y. Sun[2,b)]
[1]School of Engineering, Penn State Erie, The Behrend College, Erie, Pennsylvania 16563, USA
[2]Department of Mechanical Engineering and Mechanics, Drexel University, Philadelphia, Pennsylvania 19104, USA

(Received 29 July 2016; accepted 28 August 2016; published online 13 September 2016)

The instability of a thin liquid film on nanostructures is not well understood but is important in liquid-vapor two-phase heat transfer (e.g., thin film evaporation and boiling), lubrication, and nanomanufacturing. In thin film evaporation, the comparison between the non-evaporating film thickness and the critical film breakup thickness determines the stability of the film: the film becomes unstable when the critical film breakup thickness is larger than the non-evaporating film thickness. In this study, a closed-form model is developed to predict the critical breakup thickness of a thin liquid film on 2D periodic nanostructures based on the minimization of system free energy in the limit of a liquid monolayer. Molecular dynamics simulations are performed for water thin films on square nanostructures of varying depth and wettability, and the simulations agree with the model predictions. The results show that the critical film breakup thickness increases with the nanostructure depth and the surface wettability. The model developed here enables the prediction of the minimum film thickness for a stable thin film evaporation on a given nanostructure. *Published by AIP Publishing.*
[http://dx.doi.org/10.1063/1.4962654]

The stability of thin liquid films is important in evaporation,[1–5] boiling,[6,7] condensation,[8] lubrication,[9,10] and nanomanufacturing.[11] In particular, thin film evaporation on the nanostructured surfaces is one of the most promising thermal management solutions,[1–3] where the key challenge is to maintain a stable evaporating thin film. The breakup of the thin liquid film is detrimental to the heat transfer performance as it can lead to several orders of magnitude reduction in heat flux.

The meniscus in thin film evaporation can be divided into three regions: the non-evaporating film region, the evaporating thin film region, and the bulk meniscus. The liquid film in the first two regions experiences an excess pressure, known as the disjoining pressure that arises from long-range solid-liquid interactions, which drives the liquid flow from the bulk to the evaporating film region. The instability in thin film evaporation can be caused by (i) insufficient liquid delivery compared to evaporation and (ii) the cut-off effect of the capillary pressure (also known as the capillary wave instability[12,13]). While the former depends on the liquid delivery and evaporation rates, the latter is determined solely by the solid-liquid material system and nanostructure properties, and is thus referred to as the intrinsic instability. The evaporating meniscus is unstable if the non-evaporating film thickness is smaller than the critical film breakup thickness of the intrinsic instability. While the non-evaporating film thickness has been studied on both flat[14] and nanostructured surfaces,[15] there is a fundamental lack of understanding of the critical film breakup thickness on nanostructures.

Several models have been proposed to investigate the stability of thin liquid films. Vrij and Overbeek[12] investigated the role of surface corrugations arising from thermal fluctuations in the instability of a free standing thin liquid film. They found that corrugations with wavelengths larger than the critical wavelength grow spontaneously and cause rapid thinning and film breakup, and derived the critical wavelength by balancing van der Waals forces and surface tension forces. Majumdar and Mezic[16,17] extended the model of Vrij and Overbeek[12] for the instability of thin liquid films on an atomically smooth solid surface. Despite their proven success, these models do not account for the effect of nanostructures on film instability. Recently, Hu *et al.*[18,19] developed a closed-form model to investigate the effect of nanostructures on the meniscus shape of a thin liquid film on the nanostructured surfaces. However, this model assumes continuous meniscus shape so that it does not directly predict the critical film breakup thickness.

Molecular dynamics (MD) simulations have become a powerful tool to investigate the instability of thin liquid films. Weng *et al.*[20] studied the instability of a free standing liquid film, and analyzed the local stress profile in the thin liquid film. Maroo and Chung[21] and Seyf and Zhang[22] investigated the non-evaporating liquid film on nanostructured surfaces. While possible breakup of a non-evaporating film on the nanostructured surfaces has been shown by Maroo and Chung,[21] a continuous conformal film is obtained by Seyf and Zhang[22] in contrast. The instability of nanoscale water thin films on the methylated silica surfaces have also been recently studied.[13] However, the MD simulations are limited by the specific materials and geometries, and cannot give a general criterion for film instability.

In this letter, a general, closed-form model of the intrinsic instability of a thin liquid film on the nanostructured surfaces is developed based on the minimization of system free energy and critical condition of a monolayer liquid coverage. The MD simulations for a water-solid system are performed to verify the developed model. The effects of the nanostructure

a)L. Sun and H. Hu contributed equally to this work.
b)Author to whom correspondence should be addressed. Electronic mail: ysun@coe.drexel.edu. Tel.: +1(215)895-1373. Fax: +1(215)895-1478.

depth and wettability on the critical film breakup thickness are examined. The results are compared with the non-evaporating film thickness. The present model will be used to enable more accurate prediction of the maximum heat flux of thin film evaporation.

The schematics of a thin liquid film of thickness δ_0 on a 2D periodic nanostructured surface of wavelength L are shown in Figure 1. The basic assumptions of the model are as follows:

(i) the van der Waals interactions are the dominant solid-liquid intermolecular forces and
(ii) the meniscus shape, ζ_L, is periodic with the same wavelength of the nanostructure.

Consider a thin liquid film on a generic nanostructured surface, as shown in Fig. 1(a), the nanostructured surface is characterized with surface fluctuations of positive curvature ($\partial^2 z/\partial x^2 > 0$) and negative curvature ($\partial^2 z/\partial x^2 < 0$). Assuming the thin liquid film completely follows the profile of the solid substrate, the gradient of the capillary pressure inside the thin film drives the liquid to flow from the negative to positive curvature. As a result, the local film thickness at the location with negative curvature decreases. At the same time, decreasing local film thickness leads to a large local disjoining pressure, which prevents the liquid flow from the location of negative curvature to the location of positive curvature.

Based on the classic theory for the disjoining pressure of a thin liquid film on flat surfaces, i.e., $\Pi = A/(6\pi\delta_0^3)$,[23,24] where A is the Hamaker constant and δ_0 the liquid film thickness, as the film thickness reaches to zero, the disjoining pressure increases to infinity. However, in practice, the film thickness has a lower limit, i.e., the thickness of a monolayer, δ_m, which sets an upper bound for the disjoining pressure. Experiments have proven the validity of the classic disjoining pressure theory to the monolayer liquid coverage.[25] It is thus reasonable to assume that the disjoining pressure reaches its maximum value when the local film thickness reaches δ_m.

The critical condition that the thin liquid film breaks up occurs when the minimum local film thickness, δ^*_{min}, reaches the monolayer thickness, δ_m, following

$$\delta^*_{min}(\delta_b, \zeta_S) = \delta_m, \tag{1}$$

where δ_b is the critical film breakup thickness and ζ_S is the profile of the solid nanostructure. For the system of a thin film on a nanostructured substrate, the system free energy consists of the surface excess energy (W_γ) and van der Waals energy (W_{vdW}), where $W_\gamma = \gamma \int_{-L/2}^{L/2} [1 + [\zeta'_L(x)]^2]^{1/2} dx$ and $W_{vdW} = \frac{A}{12\pi} \int_{-L/2}^{L/2} \frac{1}{(\delta^*)^2} dx$,[18] γ is liquid surface tension, and δ^* the local film thickness, defined as the shortest distance from the meniscus to the solid surface. In equilibrium, the total system free energy reaches its minimum value, and can thus be represented with $\delta W_{total} = 0$.

Following Hu *et al.*,[18] the meniscus shape of a thin liquid film on a nanostructured surface at the critical film breakup condition can be described using a Fourier series

$$\zeta_L(x) = \sum_{n=1}^{\infty} a_n \cos\left(\frac{2\pi n}{L} x\right) + \delta_b. \tag{2}$$

Minimizing the system free system following $\delta W_{total} = (\partial W_{total}/\partial \zeta_L)\delta\zeta_L + (\partial W_{total}/\partial \zeta'_L)\delta\zeta'_L = 0$,[18] it yields

$$\int_{-L/2}^{L/2} \frac{\frac{2\pi n}{L}\sin\left(\frac{2\pi n}{L}x\right)\sum_{m=1}^{\infty} a_m \frac{2\pi m}{L}\sin\left(\frac{2\pi m}{L}x\right) dx}{\sqrt{1 + \left[\sum_{m=1}^{\infty} a_m \frac{2\pi m}{L}\sin\left(\frac{2\pi m}{L}x\right)\right]^2}} - \frac{A}{6\pi\gamma}\int_{-L/2}^{L/2} \frac{\cos\left(\frac{2\pi n}{L}x\right) dx}{[\delta^*(x)]^3} = 0. \tag{3}$$

Solving Eqs. (1)–(3) simultaneously, it gives the critical film breakup thickness, δ_b, and the Fourier coefficients, a_n, for the meniscus shape at the critical breakup condition.

Square nanostructures are commonly used in thin film evaporation experiments. Here, we investigate a thin liquid film on a steep wedge-shaped nanostructure, as shown in Fig. 1(b), to avoid having a discontinuity in the surface profile. The wedge-shaped nanostructure is characterized with the depth D, the wavelength L, and the width of the wedge, L_w. As the width of the wedge vanishes ($L_w/L \to 0$), the wedge-shaped nanostructure converges to a square nanostructure. Due to symmetry, only the left half of the nanostructure, i.e., from $x = -L/2$ to 0 is considered. The system in $[-L/2 \;\; 0]$ can be divided into four regions, where the expressions for the local film thickness are different. In region I ($x \in [-L/2, -L/4 - L_w/2]$) and region IV ($x \in [x_{III/IV}, 0]$), the local film thickness is the

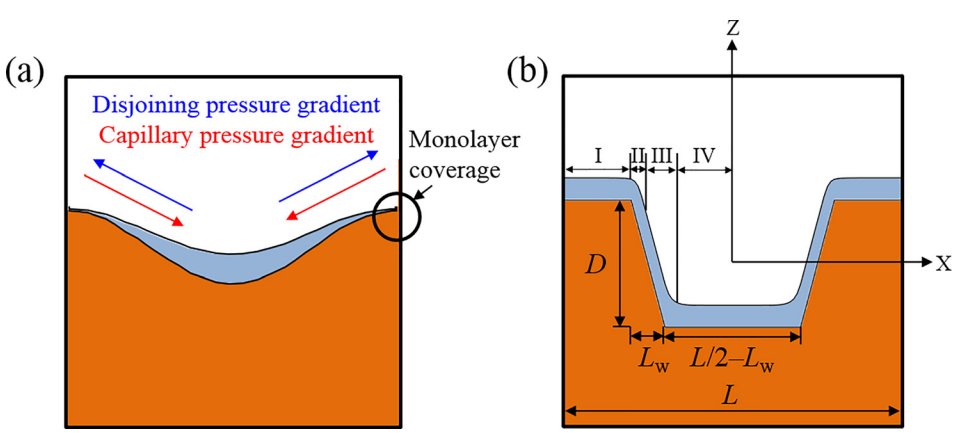

FIG. 1. (a) Schematic of the critical condition of a thin liquid film on a generic 2D nanostructured surface where the thinnest local film thickness reaches a monolayer. (b) Schematic of a 2D wedge-shaped nanostructure.

vertical distance from the meniscus to the solid surface following $\delta^*(x) = \zeta_L(x) - \zeta_S(x)$. In region II, $(x \in [-L/4 - L_w/2, x_{II/III}])$, the local film thickness is expressed as the distance from the meniscus to the edge of the nanostructure (i.e., the location with the maximum negative curvature $(-L/4 - L_w/2, D/2)$), following $\delta^*(x) = (\zeta_L(x) - \zeta_S(x))/\sqrt{(x + L/4 + L_w/2)^2 + (\zeta_L(x) - D/2)^2}$. In region III $(x \in [x_{II/III}, x_{III/IV}])$, the local film thickness is the distance from the meniscus to the solid surface along the normal direction of the solid surface following $\delta^*(x) = \sqrt{(Dx + DL/4 + L_w\zeta_L(x))^2/(D^2 + L_w^2)}$. The continuity of the meniscus shape requires $\delta^*_{II}(x_{II/III}) = \delta^*_{III}(x_{II/III})$ and $\delta^*_{III}(x_{III/IV}) = \delta^*_{IV}(x_{III/IV})$, based on which $x_{II/III}$ and $x_{III/IV}$ can be calculated.

As discussed earlier, the minimum film thickness occurs at the location of the maximum negative curvature, i.e., at $x = \pm(L/4 + L_w/2)$ for the wedge-shaped nanostructure. Using Eqs. (1) and (2), it yields

$$\sum_{n=1}^{\infty} a_n \cos\left(\frac{2\pi n}{L}\left(\frac{L_w}{2} + \frac{L}{4}\right)\right) + \delta_b - \frac{D}{2} = \delta_m. \quad (4)$$

For a wedge-shaped nanostructure with a given depth D, wavelength L, and Hamaker constant A, the critical film breakup thickness, δ_b, as a function of wedge width L_w can be calculated by solving Eqs. (2)–(4). The critical film breakup thickness for a square nanostructure with depth D and wavelength L can hence be determined by extrapolating the calculated δ_b for wedge-shaped nanostructures in the limit of $L_w/L \to 0$.

In order to verify the model-predicted critical film breakup thickness, molecular dynamics simulations were performed for water thin films on square nanostructures of varying depth and wettability. The details of the simulation setup and methodology can be found in our earlier work.[18] The wavelength of the nanostructure, L, was fixed at 22.84 nm. The nanostructure depth, D, was varied from 0, 2.86, 5.71, and 8.57 to 11.42 nm. Periodic boundary conditions were applied in all directions. Two atomic layers of solid were frozen at the bottom of the nanostructure in the z direction. As the chosen force fields may significantly affect the MD results,[26–28] we applied the force fields that have been shown to produce accurate interfacial properties. The TIP4P-Ew water model[29] that accurately describes water surface tension was used to describe the interactions between water molecules, the embedded-atom model (EAM) that accurately captures the solid surface energy[30] was used for the solid and a standard 12–6 Lennard-Jones potential was used to describe the water-solid interactions. The possible electrostatic interactions between water and solid surfaces due to the polarity of water molecules[31] were not accounted for. All simulations performed using Large-scale Atomic/Molecular Massively Parallel Simulator (LAMMPS)[12] in an NVT (N the number of atoms, V the volume, and T the temperature) ensemble at 300 K until the system reached equilibrium with a time step of 1 fs.

The lower and upper bounds of the critical film breakup thickness δ_b can be directly obtained from the MD simulations.[32] The lower bound of the critical film thickness, $\delta_{b,low}$, is the maximum film thickness that leads to film breakup. The higher bound of the critical film thickness, $\delta_{b,high}$, is the minimum film thickness that ensures a continuous film. The critical film breakup thickness should lie between $\delta_{b,low}$ and $\delta_{b,high}$. Figure 2 shows the MD results for film instability on a nanostructured surface of depth $D = 5.71$ nm and scaled Hamaker constant $A/A_0 = 0.25$, where liquid films of thickness below 1.18 nm always break up and films of thickness above 1.25 nm always stable, resulting in the lower and upper bounds of the critical film breakup thickness of $\delta_{b,low} = 1.18$ nm and $\delta_{b,high} = 1.25$ nm, respectively.

The wettability of the nanostructures was controlled by altering the Hamaker constant of the solid-liquid-vapor system. Figure 3 shows the equilibrium water contact angle as a function of the scaled Hamaker constant. For each Hamaker constant, the equilibrium contact angle was determined by performing MD simulations of droplet spreading[33] (setup shown in the inset of Fig. 3(a)). The Hamaker constant based on the water-gold Lennard-Jones potential is $A_0 = 7.19 \times 10^{-19}$ J,[31] which yields an equilibrium contact angle of 3.3°. The scaled Hamaker constant, A/A_0, represents the strength of the solid-liquid interactions relative to the water-gold interactions. As shown in Fig. 3(a), the equilibrium contact angle increases from 3.3° for $A/A_0 = 1.0$, 11° for $A/A_0 = 0.5$, 19° for $A/A_0 = 0.25$, 55° for $A/A_0 = 0.2$, to 111° for $A/A_0 = 0.1$. The MD simulations were also performed to calculate the monolayer thickness of water adsorbed on solid surfaces for varying scaled Hamaker constant, as shown in Fig. 3(b). The monolayer thickness was calculated as the thickness of the first layering of water, i.e., the distance from the solid surface to the first valley of the 1D water density profile on a solid surface (see the inset of Fig. 3(b)). As shown in Fig. 3(b), the monolayer thickness of water decreases rapidly with the scaled Hamaker constant. The MD-determined liquid monolayer thickness is substituted into our model (Eqs. (2)–(4)) to calculate the critical film breakup thickness.

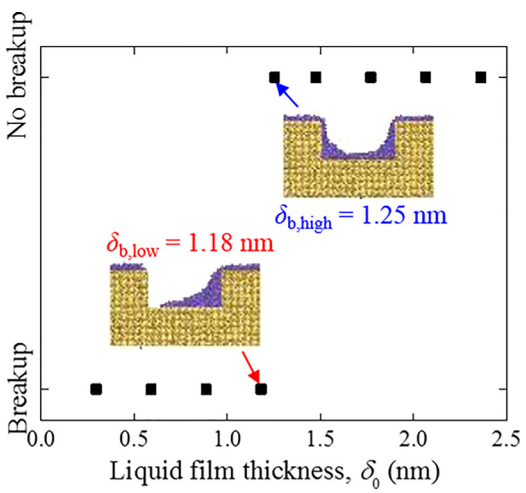

FIG. 2. The MD results for film instability of water thin films on a square gold nanostructure with 5.71 nm depth and scaled Hamaker constant of $A/A_0 = 0.25$. The inset shows the MD snapshots for the lower and upper bounds of the critical film breakup thickness.

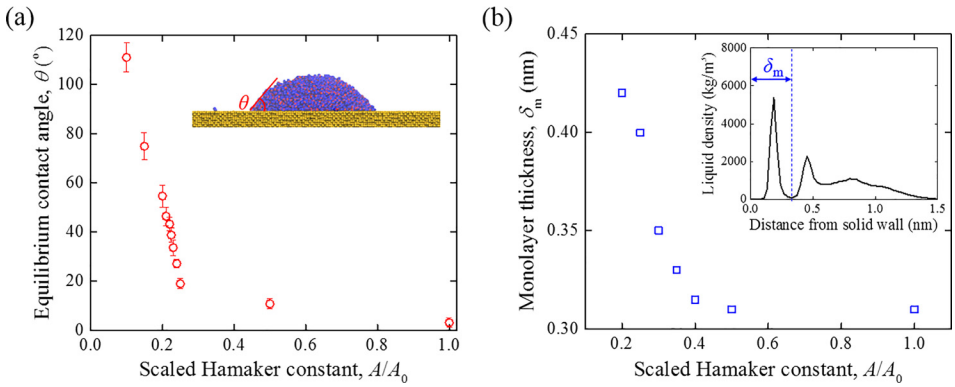

FIG. 3. (a) Equilibrium contact angle, θ, and (b) liquid monolayer thickness, δ_m, as a function of the scaled Hamaker constant, A/A_0. The inset of (a) shows the MD setup of water spreading on a flat solid surface for equilibrium contact angle measurement. The inset of (b) shows the definition of liquid monolayer thickness based on the 1D density profile of liquid on a solid surface.

Figure 4 shows the comparison between the MD-determined and model-predicted scaled critical film breakup thickness, δ_b/r, as a function of the scaled Hamaker constant, A/A_0, for thin liquid films on square nanostructures with the depth of 2.85 nm, 5.71 nm, 8.57 nm, and 11.42 nm. The critical film breakup thickness is scaled with the Wenzel roughness ratio, which is the ratio of the actual and flat surface areas and for a square nanostructure of depth D and wavelength L, $r = 1 + 2D/L$. The dashed lines in Fig. 4 represent the prediction of the closed-form model and the symbols are for MD results. The MD results agree qualitatively with the model predictions, both of which show that the critical film breakup thickness increases rapidly with decreasing scaled Hamaker constant. As the Hamaker constant decreases, the solid surface becomes more hydrophobic (see Fig. 3(a)) and the solid-liquid interactions become weaker. As a result, the liquid-vapor surface tension forces are stronger relative to the solid-liquid van der Waals interactions, making the film unstable. It is also observed that the model predictions for the scaled critical film breakup thickness, δ_b/r, versus the scaled Hamaker constant collapse to a master curve, suggesting that $\delta_b \sim r$.

In order to better understand how the intrinsic instability of thin liquid films affects thin film evaporation, the scaled non-evaporating film thickness is also plotted in Fig. 4. The non-evaporating film thickness is calculated based on our

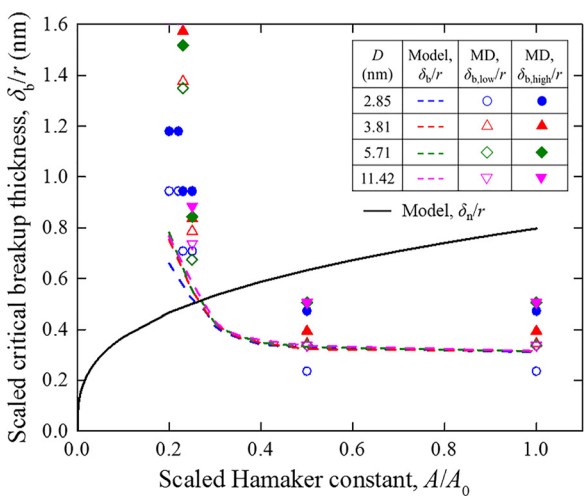

FIG. 4. Comparison between MD simulated and model predicted critical film breakup thickness, δ_b, as a function of the scaled Hamaker constant, A/A_0, for water thin films on square gold nanostructures of varying depth, together with the model-predicted non-evaporating film thickness, δ_n, under a superheat of 15 K.

early thin film evaporation model on the nanostructured surfaces in the limit of completely suppressed evaporation,[15] which follows

$$\delta_n = r\left(\frac{AT_v}{6\pi\rho_l h_{fg}(T_s - T_v)}\right)^{1/3}, \tag{5}$$

where h_{fg} is the enthalpy of evaporation, ρ_l is the liquid density, T_v is the vapor temperature, and $(T_s - T_v)$ is the superheat. In the limit of a flat surface, the Wenzel roughness ratio $r = 1$, and Eq. (5) reduces to the prediction of Wayner *et al.* for non-evaporating film thickness on a planar surface.[14] In Fig. 4, the black solid line shows the scaled non-evaporating film thickness under a superheat of 15 K using Eq. (5). It is important to note that the evaporating meniscus is stable when the non-evaporating film thickness is greater than the critical film breakup thickness (i.e., $\delta_n > \delta_b$), but breaks up when $\delta_n < \delta_b$. As shown in Fig. 4, as the scaled Hamaker constant decreases, the scaled non-evaporating film thickness decreases, but the scaled critical film breakup thickness increases. Therefore, to maintain a stable evaporating thin film, surfaces with higher Hamaker constant (i.e., more hydrophilic surfaces) are preferred in thin film evaporation. In addition, larger nanostructure depth leads to the increase in both δ_b and δ_n. Based on Eq. (5), the non-evaporating film thickness increases linearly with the Wenzel roughness ratio, i.e., $\delta_n \sim r$. As discussed earlier, the critical film breakup thickness also follows $\delta_b \sim r$. Therefore, while keeping everything else identical, changing the nanostructure depth alone does not affect the competition between δ_b and δ_n.

In this letter, a closed-form model is derived to predict the critical breakup thickness of a thin liquid film on a nanostructured surface based on minimization of the system free energy in the limit of a liquid monolayer. Molecular dynamics simulations of water thin films of varying thickness on a square gold nanostructure of varying depth and wettability are performed to verify the model with the qualitative agreement. The results show that the critical film breakup thickness increases with the nanostructure depth, following $\delta_b \sim r$, where r is the Wenzel roughness ratio. For a given nanostructure depth, the critical film thickness becomes smaller on a more hydrophilic surface due to stronger solid-liquid interactions. When the non-evaporating film thickness, δ_n, is larger than the critical film breakup thickness, δ_b, the evaporating meniscus is stable. But the evaporating meniscus breaks up when $\delta_n < \delta_b$. In thin film evaporation, to ensure a stable liquid film, substrates with a higher Hamaker constant are preferred.

The model developed here enables the prediction of the minimum film thickness for a stable thin film evaporation on a given nanostructure. Integrating with the thin film evaporation model of a nanostructure, the present model will enable more accurate prediction of maximum heat flux of an evaporating meniscus.

The support for this work was provided by the U.S. National Science Foundation (Nos. DMR-1104835 and CMMI-1401438). Computational resources were provided by the Extreme Science and Engineering Discovery Environment (XSEDE) (Grant No. TG-CTS110056).

[1]H. Wang, S. V. Garimella, and J. Y. Murthy, Int. J. Heat Mass Transfer **50**, 3933 (2007).
[2]A. J. Jiao, H. B. Ma, and J. K. Critser, Int. J. Heat Mass Transfer **50**, 2905 (2007).
[3]J. L. Plawsky, A. G. Fedorov, S. V. Garimella, H. B. Ma, S. C. Maroo, L. Chen, and Y. Nam, Nanoscale Microscale Thermophys. Eng. **18**, 251 (2014).
[4]S. Narayanan, A. G. Fedorov, and Y. K. Joshi, Int. J. Heat Mass Transfer **58**, 300 (2013).
[5]R. Xiao, S. C. Maroo, and E. N. Wang, Appl. Phys. Lett. **102**, 123103 (2013).
[6]V. P. Carey, Exp. Heat Transfer **26**, 296 (2013).
[7]S. G. Kandlikar, Exp. Therm. Fluid Sci. **26**, 389 (2002).
[8]A. V. Neimark and P. I. Ravikovitch, Microporous Mesoporous Mater. **44–45**, 697 (2001).
[9]A. R. Mendez and D. B. Bogy, Tribol. Lett. **61**, 22 (2016).
[10]C. M. Mate, Tribol. Lett. **51**, 385 (2013).
[11]K. Fukuzawa, T. Deguchi, Y. Yarnawaki, S. Itoh, T. Murarnatsu, and H. Zhang, Langmuir **24**, 2921 (2008).
[12]A. Vrij and J. T. G. Overbeek, J. Am. Chem. Soc. **90**, 3074 (1968).
[13]J. Zhang, W. Li, Y. Yan, Y. Wang, B. Liu, Y. Shen, H. Chen, and L. Liu, Phys. Chem. Chem. Phys. **17**, 451 (2015).
[14]P. C. Wayner, Jr., Y. K. Kao, and L. V. LaCroix, Int. J. Heat Mass Transfer **19**, 487 (1976).
[15]H. Hu and Y. Sun, Int. J. Heat Mass Transfer **101**, 878 (2016).
[16]A. Majumdar and I. Mezic, Microscale Thermophys. Eng. **2**, 203 (1998).
[17]A. Majumdar and I. Mezic, J. Heat Transfer **121**, 964 (1999).
[18]H. Hu, C. R. Weinberger, and Y. Sun, Nano Lett. **14**, 7131 (2014).
[19]H. Hu, C. R. Weinberger, and Y. Sun, J. Phys. Chem. C **119**, 11777 (2015).
[20]J. G. Weng, S. Park, J. R. Lukes, and C. L. Tien, J. Chem. Phys. **113**, 5917 (2000).
[21]S. C. Maroo and J. N. Chung, J. Heat Transfer **135**, 041501 (2013).
[22]H. Reza Seyf and Y. Zhang, J. Heat Transfer **135**, 121503 (2013).
[23]H. C. Hamaker, Physica **4**, 1058 (1937).
[24]J. N. Israelachvili, *Intermolecular and Surface Forces* (Academic, Burlington, MA, 2011).
[25]V. Panella, R. Chiarello, and J. Krim, Phys. Rev. Lett. **76**, 3606 (1996).
[26]S. M. Rassoulinejad-Mousavi, Y. Mao, and Y. Zhang, J. Appl. Phys. **119**, 244304 (2016).
[27]Z. T. Trautt, F. Tavazza, and C. A. Becker, Modell. Simul. Mater. Sci. Eng. **23**, 074009 (2015).
[28]C. A. Becker, F. Tavazza, Z. T. Trautt, and R. A. B. de Macedo, Curr. Opin. Solid State Mater. Sci. **17**, 277 (2013).
[29]H. W. Horn, W. C. Swope, J. W. Pitera, J. D. Madura, T. J. Dick, G. L. Hura, and T. Head-Gordon, J. Chem. Phys. **120**, 9665 (2004).
[30]S. Foiles, M. Baskes, and M. S. Daw, Phys. Rev. B **33**, 7983 (1986).
[31]H. Hu and Y. Sun, Appl. Phys. Lett. **103**, 263110 (2013).
[32]L. Sun and J. Zhou, in ASME 2015 13th International Conference on Nanochannels, Microchannels, and Minichannels, San Francisco, CA (2015).
[33]H. Hu, H.-F. Ji, and Y. Sun, Phys. Chem. Chem. Phys. **15**, 16557 (2013).